Intermetallics 94 (2018) 65–72

Contents lists available at ScienceDirect

Intermetallics

journal homepage: www.elsevier.com/locate/intermet

Effects of Ni-P amorphous films on mechanical and corrosion properties of $Al_{0.3}CoCrFeNi$ high-entropy alloys

Z.H. Xia[a], M. Zhang[a,b], Y. Zhang[c], Y. Zhao[d], P.K. Liaw[e], J.W. Qiao[a,b,*]

[a] Research Center for High-entropy Alloys, College of Materials Science and Engineering, Taiyuan University of Technology, Taiyuan 030024, China
[b] Key Laboratory of Interface Science and Engineering in Advanced Materials, Ministry of Education, Taiyuan University of Technology, Taiyuan 030024, China
[c] State Key Laboratory for Advanced Metals and Materials, University of Science and Technology Beijing, Beijing 100083, China
[d] National Key Laboratory for Remanufacturing, Academy of Armored Forces Engineering, Beijing, 100072, China
[e] Department of Materials Science and Engineering, The University of Tennessee, Knoxville, TN 37996-2200, USA

ARTICLE INFO

Keywords:
High-entropy alloy
Ni-P amorphous films
Mechanical property
Shear bands
Corrosion resistance

ABSTRACT

Through electroless plating, the $Al_{0.3}CoCrFeNi$ high-entropy alloys were successfully coated with the Ni-P amorphous film with a thickness of 1.2 μm. For studying the surface change of samples after chemical plating, the surface morphologies of the as-cast HEA substrate and HEA with the Ni-P film were contrasted by atomic-force microscopy. The tensile properties of the samples with and without the Ni-P film, and the deformational behavior of thin Ni-P film were researched, respectively. In addition, the effect of the Ni-P amorphous film on corrosion resistance of the coated HEAs was also investigated. The experimental results show that in contrast to the uncoated samples with a yielding strength of 275 MPa, the yielding strength of the coated samples exhibits 400 MPa, with a 45% improvement, which can be attributed to the very high yield strength of the Ni-P amorphous film. A tensile strain up to 10% was achieved in the Ni-P film since the propagation of one primary shear band was inhibited, and the stress/strain concentration was retarded by the plastic substrate. The corrosion resistance of the HEA with the Ni-P film is superior to that of the bare HEA in the 3.5 wt percent NaCl solutions due to the chemical homogeneity and the absence of microscopic defects in the Ni-P amorphous film. The current results indicate that the surface coating is an effective means for optimizing the properties of HEAs, and the thin Ni-P coating can remarkably improve the strength of the present HEAs.

1. Introduction

High-entropy alloys (HEAs), originally based on the novel alloy-design philosophy of mixing five or more elements in equiatomic or near-equiatomic proportions, have proven to be a promising class of materials [1–3]. Massive research has been carried out to study HEAs, and many alloy systems have been developed for their excellent properties [4–6], such as high strength and hardness [7], exceptional ductility and fracture toughness as well as superparamagnetism that provide great potential for various industrial applications [8,9]. According to traditional existing knowledge of physical metallurgy and phase diagrams, multicomponent alloys may be more inclined to develop a great variety of complex and brittle intermetallic phases that are not conductive to analyze and design. However, what is surprising is that the high mixing entropy in these alloys promotes the formation of single body-centered cubic (bcc), face-centered cubic (fcc), or hexagonal close-packed (hcp) solid-solution phases with simple structures and thereby decreases the number of phases, which provide them with many unusual performance [9].

From the mechanical-properties perspective, it is already known that in general, the single-phased bcc-structured HEAs have limited ductility [4,10], while single-phased fcc structured HEAs could have high ductility but their strength is low [11–13]. Therefore, how to fabricate the HEAs with both high strength and high ductility is a challenging topic during its research and development. In recent years, numerous efforts have been devoted to improving the strength of HEAs, and many significant progresses have been made. For instance, after the annealing heat treatment at 750 °C, the yield stress of the $CoCrFeNiNb_{0.25}$ HEAs with good ductility is almost doubled due to the strengthening of a lath-shaped fcc precipitates with nano basket-weaves microstructures [14]. The eutectic $CoCrFeNiNb_{0.5}$ HEAs, composed of a ductile fcc phase and a hard Laves phase and prepared by He et al. [15] on the basis of the computer-aided thermodynamic calculations, display an unprecedented combination of the compressive fracture strength and strain up to 2300 MPa and 23.6%, respectively. Meanwhile, by decreasing the Mo and W contents to 0.8 in the $Co_2Mo_xNi_2VW_x$ alloy,

* Corresponding author. Research Center for High-entropy Alloys, College of Materials Science and Engineering, Taiyuan University of Technology, Taiyuan 030024, China.
E-mail address: qiaojunwei@tyut.edu.cn (J.W. Qiao).

https://doi.org/10.1016/j.intermet.2017.12.021
Received 14 October 2017; Received in revised form 8 December 2017; Accepted 19 December 2017

Jiang et al. [16] obtained a fully-eutectic HEA that exhibited a high compression strength of 2364 MPa. In addition, Wang et al. [17] employed the cold rolling to break down the as-cast dendrite microstructure of the $Al_{0.25}CoCrFe_{1.25}Ni_{1.25}$ HEAs, and with increasing the thickness reduction from cold rolling, the hardness, yielding strength, and fracture strength increased at the cost of reducing ductility. He et al. [18] also demonstrated that the properties of the fcc-HEA systems could be manipulated using integrated strengthening approaches.

Furthermore, some unique approaches have been utilized to treat as-prepared alloys for optimizing their mechanical properties through surface modification [19,20]. Surface coating, one of surface modifications, is recently considered to be a valid technique to enhance the ductility of metallic glass, owing to the important role of coating in confining the propagation of shear bands [21]. Hence, thin coatings and the corresponding preparation methods should receive enough attention. In the present study, the Ni-P amorphous coating is successfully deposited on the $Al_{0.3}CoCrFeNi$ HEA substrate by electroless plating, and the effects of the Ni-P coating on the mechanical and corrosion properties of substrates have been researched.

2. Experimental

The HEAs, with the nominal composition of $Al_{0.3}CoCrFeNi$, were prepared by arc-melting a mixture of Al, Co, Cr, Fe, and Ni elementary substances with purities greater than 99.9 wt% in a Ti-gettered high purity-argon atmosphere, and re-melting at least four times to ensure homogeneity. The master ingots were, then, drop-casted into a copper mold with a dimension of $85 \times 10 \times 2\,mm^3$. Dog bone-shaped platy tensile samples, with a gauge length of 10 mm and a width of 2 mm, were cut from the as-cast sample using a wire-cut electric-discharge machine. The as-cast HEA samples, used as the substrate, were firstly grinded by fine sandpapers and mechanically-polished to make a relatively-smooth surface, which might contribute to improving the binding strength between the Ni-P coating and HEA substrate. Then, these polished specimens with a final thickness of 1.80 mm were separately washed by ultrasonic cleaning with ethanol and acetone for the purpose of removing the surface grease of the substrate. Prior to chemical plating, the cleaned samples were activated by chemistry.

After the pretreatment, the samples were immersed into the electroless plating solution which consists of the 25 g/l nickel sulfate, 25 g/l sodium hypophosphite, 10 g/l ammonium bifluoride, 4 g/l sodium hydroxide, 20 g/l citric acid, 10 ml/l hydrofluoric acid, and 1 mg/l thiourea. The pH value of the plating solution, which was measured by a PH-100 model pH meter with an accuracy of ± 0.02, was adjusted to 6.0–6.5 with a moderate-aqueous ammonia solution. The temperature of the plating solution was maintained at 80–90 °C during plating. The plating process lasted for 30 min.

Uniaxial tensile tests were carried out on an Instron 5969 material machine at room temperature and with a strain rate of $1 \times 10^{-3}\ s^{-1}$. The coated samples, subjected to different strain, were examined by the scanning-electron microscope (SEM) after tensile tests. In order to measure the thin-film thickness, the cross-sectional microstructure of the coated sample before tensile deformation was also examined by SEM. The phase structures of the HEA substrates and Ni-P films were examined by X-ray diffraction (XRD). Chemical compositions of the coating were determined, using an energy-dispersive spectrometer (EDS). A nano-indentation test was performed to measure the elasticity modulus of the HEA substrate. Atomic force microscopy (AFM) was employed to obtain the surface morphology and average roughness of specimens before and after coating, respectively. The corrosion resistance of the samples with or without the Ni-P film was studied by a CS350 electrochemical-measurement system in a 3.5 wt% NaCl solution at room temperature. The rod samples with a diameter of 3 mm were cut into 5 mm in length and then mechanically polished carefully. For electrochemical testing, the samples were electrically connected to an isolated copper wire and embedded in the epoxy resin so that only the polished surface of the cross-sectional area was exposed in the aqueous solution. The electrochemical measurements were conducted in a three-electrode cell, a saturated calomel electrode was used as the reference electrode and platinum as the counter electrode. Potentiodynamic-polarization curves were obtained with a potential sweep rate of 1 mV/s, when the open-circuit potential became almost steady.

3. Results

During the electroless plating, there are some reactions maintaining the Ni-P codeposition, which is considered as autocatalytic oxidation process. According to the hydrogen free radical theory, the surface nickel atoms coming from HEA substrate act as the reaction catalyst. The first step is that $H_2PO_2^-$ ions are reacted with H_2O molecule to produce hydrogen free-radical in the presence of catalyst and water-bath heating, as shown in Eq. (1). Due to their high energy and chemical activity, then, these free radicals are unstable and liable to have reaction with Ni^{2+} ions in the solution, producing Ni atoms adsorbed on the surface of substrate, as shown in Eq. (2). Meanwhile, as shown in Eq. (3), the $H_2PO_2^-$ ions can also react with hydrogen free radicals to produce the P atoms. It is worth noting that the Ni atoms, provided by Ni-P film rather than HEA substrate, act as the catalyst triggering oxidation reaction of sodium hypophosphite after the substrate was plated with a thin layer of Ni-P alloy, thus promoting the chemical nickel-plating. The main chemical equation during the electroless deposition are as follows:

$$H_2PO_2^- + H_2O \xrightarrow[\text{Heating}]{\text{Ni}} HPO_3^{2-} + 2H\cdot + H^+ \quad (1)$$

$$Ni^{2+} + 2H\cdot \rightarrow Ni + 2H^+ \quad (2)$$

$$H_2PO_2^- + H\cdot \rightarrow H_2O + OH^- + P \quad (3)$$

By Eqs. (2) and (3), which can be well described by a parallel reaction, the codeposition of Ni and P occurs sustainably, and eventually forms a Ni-P coating on the surface of HEA substrate.

3.1. Microstructure of the samples

Fig. 1a shows the sandwich structure consisting of the protecting coating, 1.2-μm-thick Ni-P amorphous film, and $Al_{0.3}CoCrFeNi$ HEA substrate. It can be seen that there is a clear and straight interface between the Ni-P coating and HEA substrate, basically suggesting that the

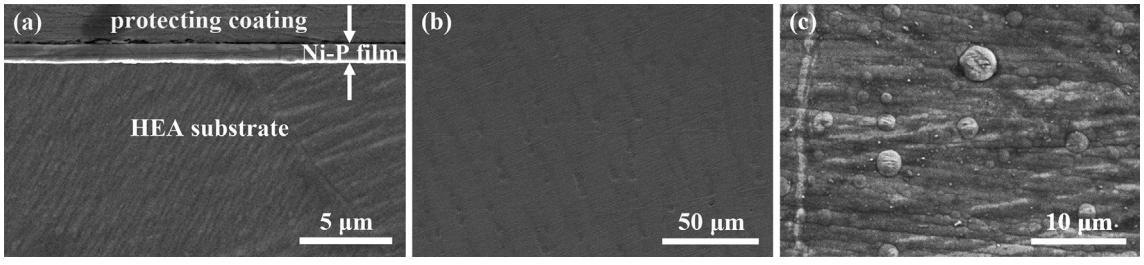

Fig. 1. (a) Cross-sectional SEM images of the HEA substrate with the Ni-P amorphous film. SEM images of the HEA substrate (b) and Ni-P film (c).

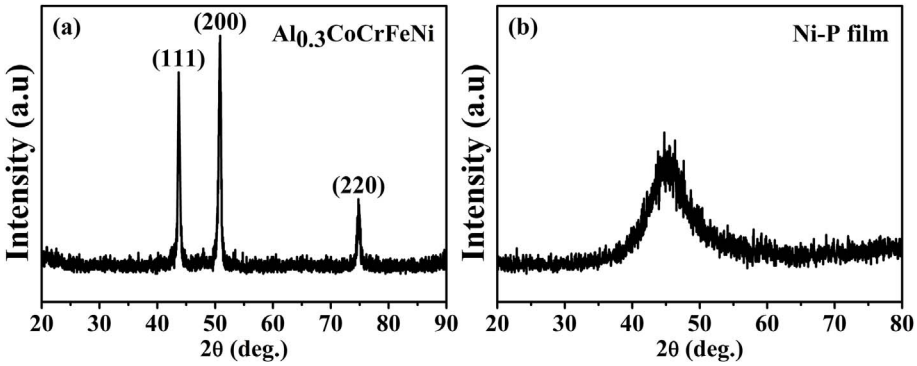

Fig. 2. XRD patterns of (a) HEA substrate and (b) surface Ni-P film.

coating has a better adhesion with the HEA substrate. Along the coating extension, it can be found that the Ni-P film, which are prepared by electroless plating, is uniform, and no microcracks can be observed. The SEM images of the HEA substrate and Ni-P film are shown in Fig. 1b and c, respectively. From Fig. 1b, one can see that the dendrite size of the HEA substrate has a narrow distribution ranging from 10 to 20 μm. As shown in Fig. 1c, the surface cell-shaped microstructure with various diameters may reveal an island growth mode of the amorphous film deposited on the substrate, and a similar surface morphology of Ni-P films is also reported in the previous studies [22]. In addition, the EDS analysis shows that the Ni-P films contain P content of 8.5 wt%, which is well within the range of 7–10 wt% for the composition of the amorphous film reported previously [23].

Fig. 2 presents the XRD spectra of both the HEA substrate and Ni-P film peeled from the substrate. Fig. 2a shows the XRD pattern of the HEA substrate, and sharp diffraction peaks are clearly observed, which are identified as (111), (200), and (220) planes of the FCC phase, respectively. By contrast, the spectra of the Ni-P coating, as presented in Fig. 2b, contain just a broad diffraction peak without any detectable peaks corresponding to crystalline phases, indicating that the Ni-P coatings are amorphous structure [24].

3.2. Surface roughness before and after deposition

To compare the difference of the surface topography for the HEA substrate before and after chemical deposition, AFM was applied to characterize the surface roughness of samples, and the typical morphologies are displayed in Fig. 3. Fig. 3a and b shows the obtained three-dimensional surface topographies of the uncoated and coated samples. It can be clearly seen that in contrast to the as-cast samples, the surface topography of the as-deposited samples exhibits a relatively-rough surface, signifying the increasing surface roughness of samples during electroless plating, which may be related to the above mentioned island growth mode (Fig. 1). The inset in Fig. 3b is a partial enlarged view, presenting the micro-morphology of the Ni-P film. The corresponding statistical analyses of the height values of each point for the two samples are depicted in Fig. 3c and d, respectively, and approximately shows a normal distribution on the whole. Obviously, the span of height values in Fig. 3d is larger than that in Fig. 3c, indicating that the surface of the HEA substrate has a small undulation.

On the basis of above AFM images, the roughness average (R_a) and root-mean-squares roughness (R_q) can be obtained according to the following equations:

$$R_a = \frac{1}{N}\sum_{j=1}^{N}\left|z_j\right| \tag{4}$$

$$R_q = \sqrt{\frac{\sum_{j=1}^{N} Z_j^2}{N}} \tag{5}$$

where Z_j is the height value of the AFM topography image, and N is the number of points within the image. By software calculations, the root-mean-squares roughness and roughness average for the uncoated sample are obtained to be 7.4 and 5.5 nm, respectively. And the data for the coated sample are 16.3 and 12.6 nm, respectively. It can be illustrated that the HEA substrates have a smoother surface. Fig. 3e shows that the surface height varies with the scanning distance, further verifying the smaller roughness for the HEA substrate.

3.3. Tensile properties

The typical engineering tensile curves of the samples with and without the Ni-P coating are shown in Fig. 4. For comparison, tensile behaviors of a free-standing $Ni_{80}P_{20}$ ribbon prepared by melt-spinning is also included in Fig. 4 [25]. Apparently, the ribbon shows a very high strength but almost no tensile plasticity due to their inability to suppress the formation of shear bands. The yield strength (at a 0.2% strain offset) and ultimate tensile strength of the uncoated sample are 275 MPa and 559 MPa, respectively. However, the yield strength and ultimate tensile strength of the sample coated with the Ni-P film are 400 MPa and 622 MPa, respectively, with increases of 45% in the yield strength and 11% in the ultimate tensile strength, compared with the uncoated HEA sample. In addition, it should be noticed that the elongation of the sample with the Ni-P film is 10% less than the elongation of the uncoated sample, indicating the ductility of the coated sample is primarily restricted to the HEA substrate and that the small cracks observed in the coated samples do not trigger the rupture of the entire structure. An appreciable uniform tensile strain observed in the HEA-supported thin Ni-P film was as high as 10%. Such an amazing uniform tensile ductility has rarely been reported for the amorphous alloy in the previous literature [26]. A pretty evident work hardening, comparable to the HEA substrate, arises in the main plastic-deformation process of the coated sample. This trend implies the increasing dislocation pileup and lattice friction, which are solely caused by the plastic deformation of the HEA substrate, that is to say, the existence of the Ni-P coating has little influence on strain hardening of coated samples. The inset in Fig. 4 shows the macroscopic sample geometries before and after tension. It can be seen that there is a rough surface for the fracture sample, which may be due to the local inhomogeneous deformation during tension.

3.4. The deformation behavior of Ni-P amorphous film

Tensile tests with different elongations were carried out for researching the deformational behavior of HEA-supported thin Ni-P coatings. The coated samples were stretched to a constant strain, videlicet, 5%, 10%, 20%, and 30%, respectively. Fig. 5 reveals the surface topographies of the Ni-P amorphous films subjected to different strain. The first two rows of Fig. 5 display SEM images of the coating surface with different tensile strains, and (e-h) is the enlarged view. Corresponding longitudinal-sectional SEM images are presented in (i-l). As shown in Fig. 5a-d, the larger the tensile strain of the coated sample is, the more uneven the surface of the Ni-P amorphous film is. Such a

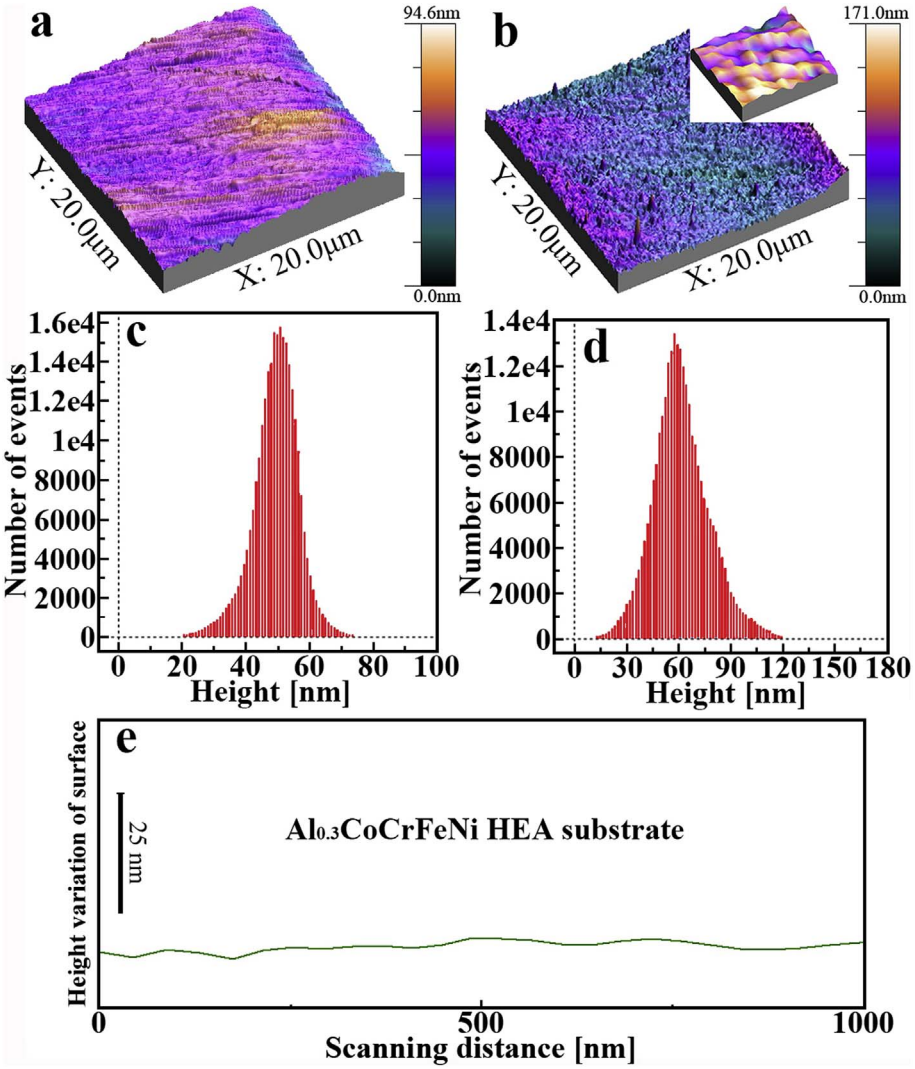

Fig. 3. The three-dimensional surface morphology of (a) HEA substrate and (b) Ni-P film. The statistical graph of values with different heights for (c) HEA substrate and (d) Ni-P film. (e) The height variations of the HEA substrate surface.

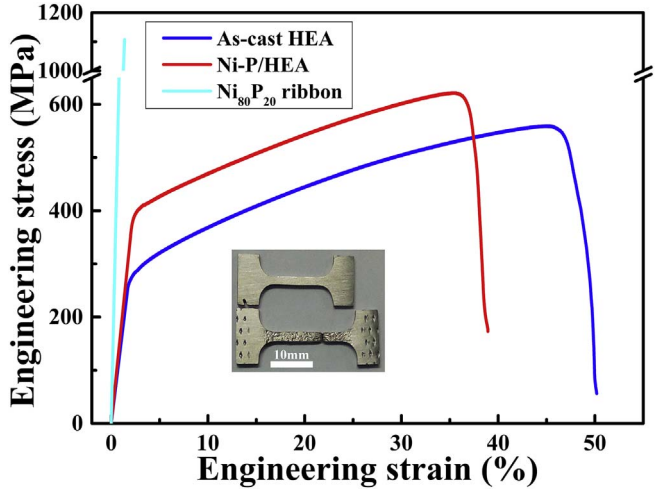

Fig. 4. Tensile engineering stress-strain curves of as-cast and Ni-P-coated HEAs. For comparison, the stress-strain curve of the free-standing Ni80P20 is also included.

phenomenon is mainly due to the rough surface of the HEA substrate after tension. No obvious surface crack except few shear bands was observed in the Ni-P film when the elongation is less than 10%, as shown at low magnification (Fig. 5a and b). With the increase of the tensile strain, the distribution of the shear-banding relative density gradually becomes uniform, and the quantity is gradually increasing. Dense multiple shear bands were exposed under the high magnification (Fig. 5e–h). Furthermore, a limited number of cracks can be observed on the SEM surface images of the Ni-P film while the engineering strain is below 10%. What is noteworthy is that aforesaid cracking may result from the locally-larger strain in the HEA substrate beneath the film during tension. The enlarged SEM image of the film surface in Fig. 5g shows large cracks that propagated obliquely at the certain angle to the tensile direction. In addition, as indicated by the dashed line in Fig. 5h, numerous cracks induced by shear bands with an angle of ~45° to the depth direction and secondary shear bands stimulated by the main shear bands are observed in the Ni-P film. Fig. 5(i–l) show the longitudinal section of Ni-P films on the HEA substrate with different tensile strains. It can be seen that the film thickness has a slight reduction with increasing the tensile strain. This result confirms that there may be a non-localized plastic deformation for Ni-P films during tension. By checking the fracture in the longitudinal-sectional image, it can be found that the fracture type of the amorphous films is not a cleavage but shearing, as indicated by dashed circles in Fig. 5l, suggesting that Ni-P films achieve a large elongation [26]. Additionally, although the tensile strain reached 30%, the Ni-P amorphous film still did not flake off from HEA substrate. The results provide an obvious fact that the interface between the substrate and Ni-P film has a strong bond.

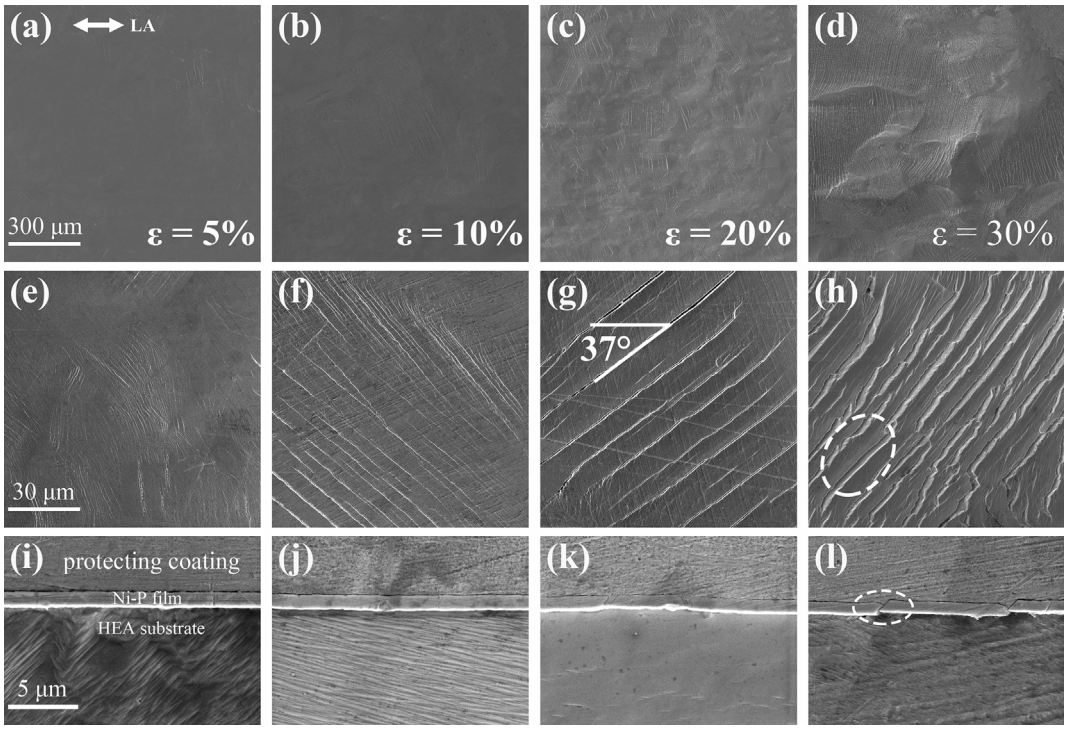

Fig. 5. SEM images of the amorphous film surface with the tensile strains of 5% (a, e), 10% (b, f), 20% (e, g), and 30% (d, h). (e–h) is magnified images. (i–l), Transverse-sectional SEM images with strain of 5% (i), 10% (j), 20% (k), and 30% (l). LA indicates the loading axis in tensile tests.

3.5. Corrosion behavior of samples

It has been reported that Ni-P amorphous coatings could be applied to improve the corrosion resistance for conventional crystal alloys, such as aluminum alloys [27]. In the current study, the effect of Ni-P films on the corrosion resistance of the coated HEAs has been investigated. Fig. 6 shows the representative potentiodynamic-polarization curves and impedance diagram of as-cast HEAs and HEAs with the Ni-P coating in the 3.5 wt% NaCl solutions at room temperature, respectively. As shown in Fig. 6a, the corrosion behavior of both samples is nearly similar in the NaCl solutions. In the initial stage of the anode-polarization curve, the corrosion current densities for these samples exhibit a rapid increase, indicating an active dissolution state at the beginning of corrosion. With the increasing potential, a typical passivation behavior appears in both samples. The remarkably sharp rise of the current density occurs when up to around 0.13 V for the uncoated sample and 0.35 V for the coated sample, which might be related to the dissolution of the passivation film formed on the surface. Further, it implies that the pitting caused by the chloride ion may occur on the sample surfaces at this polarization potential. Moreover, it is noted that even though there may also be pitting corrosion on the surface for the coated samples, the pitting potential of the coated samples is higher than that of the uncoated samples. This trend indicates that the Ni-P amorphous coating is superior to the HEA in terms of the pitting-resistance property. The corresponding corrosion potential (E_{corr}) for the uncoated and coated samples are - 0.218 V and - 0.148 V, respectively. The lower E_{corr} value of the uncoated sample suggests that in contrast to the coated sample, the uncoated sample is more liable to initiate corrosion in 3.5 wt% NaCl solutions. Generally speaking, a lower E_{corr} usually signifies that the materials have poorer chemical stability and higher corrosion tendency, while the higher corrosion current density (i_{corr}) universally implies a faster rate of corrosion. The calculation results show that compared with the 0.88 μA/cm^2 for the coated sample, the uncoated sample possesses a higher i_{corr} with a value of 1.60 μA/cm^2. Therefore, it can be concluded that the corrosion resistance of the coated sample is better than that of the uncoated sample.

Electrochemical-impedance spectroscopy (EIS) is one of the most common methods to research the anti-corrosion properties of materials.

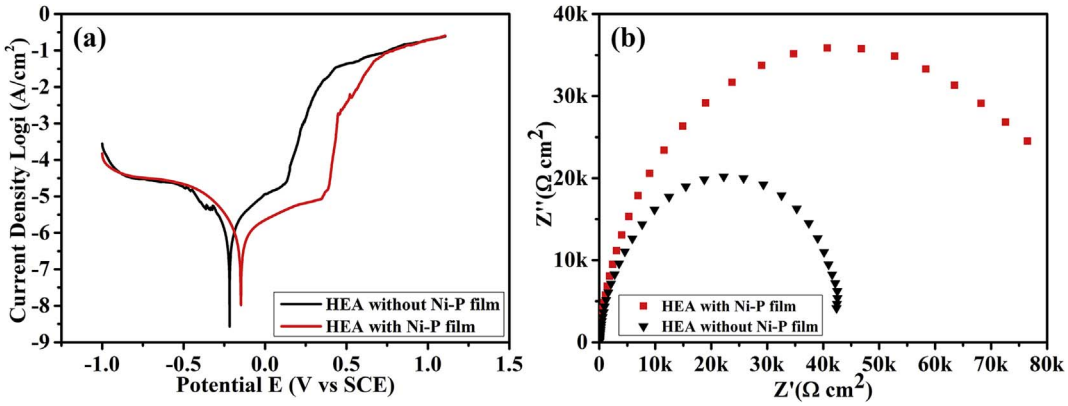

Fig. 6. (a) Potentiodynamic-polarization curves and (b) impedance diagram of as-cast HEAs and HEAs with the Ni-P coating in the 3.5 wt% NaCl solution.

The size of the impedance arc is generally deemed as a good indicator for the corresponding corrosion resistance. The impedance data of two samples in 3.5 wt% NaCl solutions are shown in Fig. 6b. By comparing the size of impedance arc of the two samples, it can be readily inferred that the coated sample exhibits better corrosion resistance, which is consistent with the above results.

Taking into account the microstructure, the reason why the corrosion resistance of the HEA with the Ni-P film is superior to that of the bare HEA is that the Ni-P amorphous coating has a unique atomic arrangement with short range order and chemical homogeneity, a passive layer can be uniformly formed on the entire surface of the amorphous phase [28]. On the other hand, due to the fact that microscopic defects, such as grain boundaries and dislocations, do not exist, the fretting corrosion batteries will not be formed in the Ni-P amorphous alloy, thus increasing the chemical stability of the films in the corrosive medium. More importantly, with the corrosion running, the P element of the present amorphous films may accelerate the passivation performance of alloying elements, and promote the formation of phosphide in the corrosion environment, thereby providing the HEA substrate with an effective barrier against the active dissolution process.

4. Discussion

4.1. Amorphous film effect on yield strength

To obtain a better understanding to the strengthening mechanism of Ni-P amorphous film on the HEA substrate, a simulation based on a finite-element method (FEM) has been carried out to analyze the surface-stress distribution of the samples before and after chemical plating. The finite-element model is established with a 10 μm-thick coating tightly connected on 2 mm-thick substrate. The HEA substrate is considered as an elastic plastic solid, whose elastic properties (Young's modulus E and Poisson's ratio ν) are set to be E(HEA) = 208 GPa (measured by nanoindentation), ν(HEA) = 0.3 [29]. And the Ni-P film is simulated with an elastic-perfect-plastic body, with the yielding strength, Young's modulus, and Poisson's ratio of 1107 MPa [25], 217 GPa, and 0.37 [30], respectively. The finite-element simulation results of the sample with the Ni-P coating are shown in Fig. 7. During simulation, the displacement traction was applied along the Y-axis, while the bottom of the dummy test specimen was fixed. Only two specimen surfaces parallel to the YZ-coordinate plane were adhered with the coating so that the stress difference between the Ni-P film and HEA substrate could be clearly observed in the simulation.

It is generally acknowledged that amorphous alloys intrinsically possess a higher elastic strain than do crystalline material. According to Fig. 4, therefore, the elastic-deformation behavior of the samples with the Ni-P amorphous film is divided into two phases: elastic-elastic and elastic-plastic stages, similar to the tensile behavior of *in-situ* dendrite/metallic glass matrix composites [31]. In the first phase, both the HEA substrate and Ni-P amorphous film are mainly in the elastic state, and the coated sample is also under an elastic load. Moreover, the two sides of the bonded interface can deform synchronously due to the well-matched elasticity moduli between the substrate and the film. With further increasing the strain, the weaker substrate begins to deform plastically, while the Ni-P film still remains elastic at this stage. As a consequence, the substrate yields first on account of having a lower yield strength than the amorphous film. As shown in Fig. 7, the stress concentration is distributed on the surface of the Ni-P film rather than the HEA substrate. In other words, the existence of the amorphous film can alleviate the stress on the substrate, thus enhancing the strength for the samples with the Ni-P film.

4.2. HEA substrate induced film elongation

There is no doubt that the plasticity of the Ni-P amorphous film has a great influence on the mechanical strength for the coated sample. The smaller the elongation at the break of the HEA-supported Ni-P amorphous film is, the shorter the strengthening lasts. Therefore, only by improving the plastic-deformation ability for the amorphous film can the mechanical properties of the coated sample under tensile tests be enhanced effectively. It has been proved that the confinement by a ductile substrate is one of the useful method to increase the plasticity for brittle films [32]. For instance, Lu et al. [33] reported that Cu films deposited on a ductile polymer substrate can be stretched up to a 50% tensile strain before failure. Being subjected to the tensile test, an unaffiliated metal film tends to rupture at small strains by forming the strain localization within a narrow region. However, finite-element simulations have shown that the substrate can delocalize the strain, so that a metal film well-bonded on a polymer substrate can elongate indefinitely, but only limited by the rupture of the substrate [34]. Furthermore, a gradient nano-grained copper film, reported by Fang et al. [35], can achieve a uniform tensile strain of 31% when it is confined by a coarse-grained copper substrate. The significantly-improved compressive ductility of amorphous alloys was revealed when the strain concentration in the shear band and early cracking were suppressed by the coating [36,37]. In this study, a large tensile deformation before cracking can be achieved in the Ni-P amorphous film coated on the HEA substrate by stimulating the formation of multiple shear bands. The tensile deformation schematic for the coated samples is presented in Fig. 8, which can be used to explain the elevated plasticity of the Ni-P film. As shown in Fig. 8a, the elastic deformation mainly occurs in the Ni-P film, and the HEA substrate will deform at first elastically and then plastically before the coated sample yields. Due to the strain localization is restrained efficiently by the ductile HEA substrate, a number of shear bands, rather than the solely-primary shear band are formed in the amorphous film with the increase of the applied stress, as shown in Fig. 8b and c. Subsequently, the bonding strength of the interface between the Ni-P film and HEA substrate weaken gradually because of the local strain concentration, eventually resulting in the shear fracture of the Ni-P film, which is in good agreement with the experimental findings in Fig. 5l.

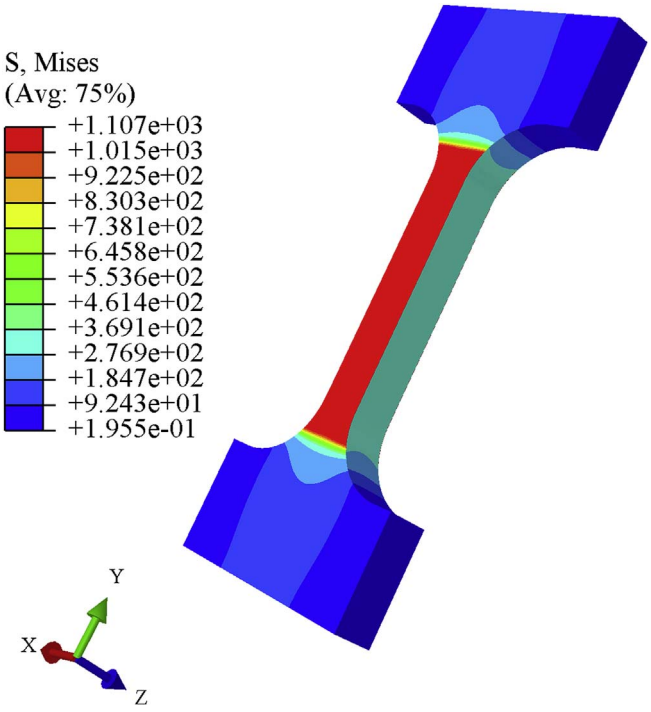

Fig. 7. The result of the simulated surface stress distribution of the coated sample.

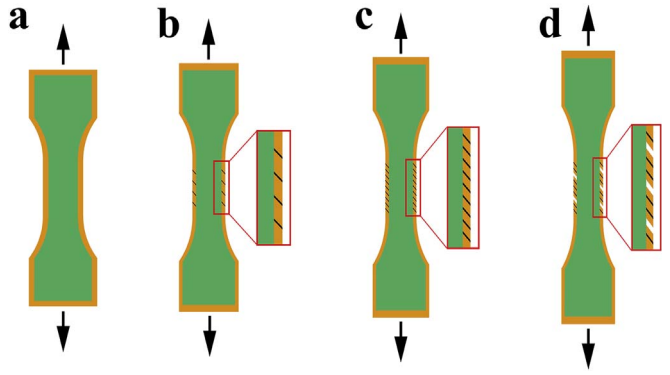

Fig. 8. Schematic of tensile deformation mechanisms for the coated samples.

4.3. Factors of influencing the strengthening

It is worth pointing out that the surface roughness and the interface-bonding strength between the Ni-P film and the substrate are two factors in improving the mechanical properties of the coated samples. The surface-roughness average of the HEA substrate before the tension test is found to be 5.5 nm, measured by AFM. A relatively-smooth interface with a small roughness between the Ni-P film and HEA substrate is also observed from SEM images, as displayed in Fig. 5i. Apparently, the smaller surface roughness of the HEA substrate will lead to a smoother interface, which in turn would effectively decrease the stress concentration and strain localization in the interface, and simultaneously reduce the possibility of debonding at the interface during tensile deformation. Moreover, if the interface possesses a poor adhesion, the HEA substrate will provide less of constraint on the Ni-P film, and a slight strain localization, triggered by the surface fluctuation, can easily cause local delamination, and the two processes promote each other thereafter, resulting in microcracks and the ultimate fracture failure of the film. As can be seen from Fig. 5k and l, however, the Ni-P amorphous film still remained well bonded with the HEA substrate without the evidently-observed delamination at the interface even at a very large tensile strain, revealing the strong binding power between the film and substrate. On the one hand, the well-bonded interface between the Ni-P film and HEA substrate insures that the film and substrate always adhered together and increases the resistance of the interface to sliding. On the other hand, it can also delocalize deformation in the film on account of the great confinement. For this reason, the Ni-P amorphous film can be stretched up to a very large elongation with little delamination since the formation of microcracks and premature fracture failure in the film can be retarded, thereby prolonging the effect of Ni-P films on the mechanical properties of HEA substrates.

5. Conclusions

In summary, the $Al_{0.3}$CoCrFeNi HEAs are successfully coated with a Ni-P amorphous film with a thickness of 1.2 μm by the electroless-plating method. The surface roughness of the as-cast HEA substrate is smaller than that of the coated HEA, which may be related to the island growth mode of the Ni-P film. In contrast to the uncoated samples with a yielding strength of 275 MPa, the yielding strength of coated sample is 400 MPa, with a 45% improvement, which can be attributed to the very high yield strength of 1107 MPa for the Ni-P amorphous film. The finite-element simulation result verifies that the existence of the amorphous film can alleviate the stress on the HEA substrate, thus enhancing the strength of the samples with the Ni-P film. A tensile strain up to 10% was achieved in the Ni-P film, since the propagation of one primary shear band was inhibited, and the stress/strain concentration was retarded by the plastic substrate. Furthermore, the smaller surface roughness and relatively strong interface-bonding force between the film and the substrate are beneficial to play the role of strengthening of Ni-P amorphous film. The corrosion resistance of the HEA with the Ni-P film is superior to that of the bare HEA in the 3.5 wt% NaCl solution due to the chemical homogeneity and the absence of microscopic defects for the Ni-P amorphous film. The current results indicate that surface coating is an effective means for optimizing the properties of HEAs, and the thin Ni-P coating can remarkably improve the strength of the present HEAs.

Acknowledgement

The authors would like to acknowledge the financial support of the Youth Natural Science Foundation of Shanxi Province, China (Nos. 2015021005), and the financial support from State Key Lab of Advanced Metals and Materials (Nos. 2015-Z07 and 2016-ZD03). Y.Z. would like thank the financial support from National Natural Science Foundation of China (NSFC), granted No. 51471025 and 51671020.

References

[1] Y.F. Ye, Q. Wang, J. Lu, C.T. Liu, Y. Yang, High-entropy alloy: challenges and prospects, Mater. Today 19 (2016) 349–362.
[2] I.S. Wani, T. Bhattacharjee, S. Sheikh, Y.P. Lu, S. Chatterjee, P.P. Bhattacharjee, S. Guo, N. Tsuji, Ultrafine-grained AlCoCrFeNi$_{2.1}$Eutectic high-entropy alloy, Mater. Res. Lett. 4 (2016) 174–179.
[3] J.W. Yeh, S.K. Chen, S.J. Lin, J.Y. Gan, T.S. Chin, T.T. Shun, C.H. Tsau, S.Y. Chang, Nanostructured high-entropy alloys with multiple principal elements: novel alloy design concepts and outcomes, Adv. Eng. Mater. 6 (2004) 299–303.
[4] O.N. Senkov, G.B. Wilks, J.M. Scott, D.B. Miracle, Mechanical properties of $Nb_{25}Mo_{25}Ta_{25}W_{25}$ and $V_{20}Nb_{20}Mo_{20}Ta_{20}W_{20}$ refractory high entropy alloys, Intermetallics 19 (2011) 698–706.
[5] Y.-F. Kao, S.-K. Chen, T.-J. Chen, P.-C. Chu, J.-W. Yeh, S.-J. Lin, Electrical, magnetic, and Hall properties of Al_xCoCrFeNi high-entropy alloys, J. Alloy. Comp. 509 (2011) 1607–1614.
[6] Z. Tang, L. Huang, W. He, P.K. Liaw, Alloying, Processing, Effects on the aqueous corrosion behavior of high-entropy alloys, Entropy 16 (2014) 895–911.
[7] O.N. Senkov, G.B. Wilks, D.B. Miracle, C.P. Chuang, P.K. Liaw, Refractory high-entropy alloys, Intermetallics 18 (2010) 1758–1765.
[8] M.-H. Tsai, J.-W. Yeh, High-entropy alloys: a Critical Review, Mater. Res. Lett. 2 (2014) 107–123.
[9] Y. Zhang, T.T. Zuo, Z. Tang, M.C. Gao, K.A. Dahmen, P.K. Liaw, Z.P. Lu, Microstructures and properties of high-entropy alloys, Prog. Mater. Sci. 61 (2014) 1–93.
[10] L. Ma, C. Li, Y. Jiang, J. Zhou, L. Wang, F. Wang, T. Cao, Y. Xue, Cooling rate-dependent microstructure and mechanical properties of $Al_xSi_{0.2}$CrFeCoNiCu$_{1-x}$ high entropy alloys, J. Alloy. Comp. 694 (2017) 61–67.
[11] C. Varvenne, A. Luque, W.A. Curtin, Theory of strengthening in fcc high entropy alloys, Acta Mater. 118 (2016) 164–176.
[12] Z.G. Zhu, K.H. Ma, Q. Wang, C.H. Shek, Compositional dependence of phase formation and mechanical properties in three CoCrFeNi-(Mn/Al/Cu) high entropy alloys, Intermetallics 79 (2016) 1–11.
[13] F. Otto, A. Dlouhý, C. Somsen, H. Bei, G. Eggeler, E.P. George, The influences of temperature and microstructure on the tensile properties of a CoCrFeMnNi high-entropy alloy, Acta Mater. 61 (2013) 5743–5755.
[14] F. He, Z. Wang, S. Niu, Q. Wu, J. Li, J. Wang, C.T. Liu, Y. Dang, Strengthening the CoCrFeNiNb$_{0.25}$ high entropy alloy by FCC precipitate, J. Alloy. Comp. 667 (2016) 53–57.
[15] F. He, Z. Wang, P. Cheng, Q. Wang, J. Li, Y. Dang, J. Wang, C.T. Liu, Designing eutectic high entropy alloys of CoCrFeNiNb$_x$, J. Alloy. Comp. 656 (2016) 284–289.
[16] H. Jiang, H. Zhang, T. Huang, Y. Lu, T. Wang, T. Li, Microstructures and mechanical properties of $Co_2Mo_xNi_2VW_x$ eutectic high entropy alloys, Mater. Des. 109 (2016) 539–546.
[17] Z. Wang, M.C. Gao, S.G. Ma, H.J. Yang, Z.H. Wang, M. Ziomek-Moroz, J.W. Qiao, Effect of cold rolling on the microstructure and mechanical properties of $Al_{0.25}$CoCrFe$_{1.25}$Ni$_{1.25}$ high-entropy alloy, Mater. Sci. Eng. A 645 (2015) 163–169.
[18] J.Y. He, H. Wang, H.L. Huang, X.D. Xu, M.W. Chen, Y. Wu, X.J. Liu, T.G. Nieh, K. An, Z.P. Lu, A precipitation-hardened high-entropy alloy with outstanding tensile properties, Acta Mater. 102 (2016) 187–196.
[19] Y. Zhang, W.H. Wang, A.L. Greer, Making metallic glasses plastic by control of residual stress, Nat. Mater. 5 (2006) 857–860.
[20] T.G. Nieh, Y. Yang, J. Lu, C.T. Liu, Effect of surface modifications on shear banding and plasticity in metallic glasses: an overview, Prog. Nat. Sci.: Mater. Int. 22 (2012) 355–363.
[21] L.W. Ren, M.M. Meng, Z. Wang, F.Q. Yang, H.J. Yang, T. Zhang, J.W. Qiao, Enhancement of plasticity in Zr-based bulk metallic glasses electroplated with copper coatings, Intermetallics 57 (2015) 121–126.
[22] J.W. Qiao, Z. Wang, L.W. Ren, H.L. Jia, S.G. Ma, H.J. Yang, Y. Zhang, Enhancement of mechanical and electrochemical properties of $Al_{0.25}$CrCoFe$_{1.25}$Ni$_{1.25}$ high-entropy alloys by coating Ni–P amorphous films, Mater. Sci. Eng. A 657 (2016) 353–358.
[23] A.W. Goldenstein, W. Rostoker, F. Schossberger, G. Gutzeit, Structure of chemically

deposited nickel, J. Electrochem. Soc. 104 (1957) 104–110.
[24] L.W. Ren, Z. Wang, M.M. Meng, H. Tian, H.J. Yang, J.W. Qiao, Plasticity enhancement in bulk metallic glasses by electroless plating with Ni-P amorphous films, J. Non-Cryst. Solids 430 (2015) 115–119.
[25] K. Ziewiec, P. Malczewski, G. Boczkal, K. Prusik, Formation and properties of amorphous/crystalline ductile composites in Ni-Ag-P Immiscible alloys, Solid State Phenom. 186 (2012) 216–221.
[26] X.L. Lu, Y. Li, L. Lu, Co-existence of homogeneous flow and localized plastic deformation in tension of amorphous Ni–P films on ductile substrate, Acta Mater. 106 (2016) 182–192.
[27] H. Yang, Y. Gao, W. Qin, Y. Li, Microstructure and corrosion behavior of electroless Ni–P on sprayed Al–Ce coating of 3003 aluminum alloy, Surf. Coating. Technol. 281 (2015) 176–183.
[28] S.J. Choi, H.S. Lee, J.W. Jang, S. Yi, Corrosion behavior in a 3.5 wt% NaCl solution of amorphous coatings prepared through plasma-spray and cold-spray coating processes, Met. Mater. Int. 20 (2014) 1053–1057.
[29] H.Y. Yasuda, K. Shigeno, T. Nagase, Dynamic strain aging of $Al_{0.3}$CoCrFeNi high entropy alloy single crystals, Scripta Mater. 108 (2015) 80–83.
[30] Akio Yonezu, Michihiro Niwa, Jiping Ye, X. Chen, Contact fracture mechanism of electroplated Ni–P coating, Mater. Sci. Eng. A 563 (2013) 184–192.
[31] J.W. Qiao, T. Zhang, F.Q. Yang, P.K. Liaw, S. Pauly, B.S. Xu, A tensile deformation model for in-situ dendrite/metallic glass matrix composites, Sci. Rep. 3 (2013) 2816.
[32] J.P. Chu, J.E. Greene, J.S.C. Jang, J.C. Huang, Y.-L. Shen, P.K. Liaw, Y. Yokoyama, A. Inoue, T.G. Nieh, Bendable bulk metallic glass: effects of a thin, adhesive, strong, and ductile coating, Acta Mater. 60 (2012) 3226–3238.
[33] N. Lu, X. Wang, Z. Suo, J. Vlassak, Metal films on polymer substrates stretched beyond 50%, Appl. Phys. Lett. 91 (2007) 221909.
[34] T. Li, Z.Y. Huang, Z.C. Xi, S.P. Lacour, S. Wagner, Z. Suo, Delocalizing strain in a thin metal film on a polymer substrate, Mech. Mater. 37 (2005) 261–273.
[35] T.H. Fang, W.L. Li, N.R. Tao, K. Lu, Revealing extraordinary intrinsic tensile plasticity in gradient nano-grained copper, Science 331 (2011) 1587–1590.
[36] L.W. Ren, F.Q. Yang, Z.M. Jiao, H.J. Yang, Z.H. Wang, J.W. Qiao, Plasticity enhancement in Ni–P amorphous alloy/Ni/Zr-based metallic glass composites with a sandwich structure, Mater. Sci. Eng. A 643 (2015) 175–182.
[37] J.W. Cao, J.G. Han, Z.H. Guo, W.B. Zhao, Y.Q. Guo, Z.H. Xia, J.W. Qiao, Plasticity enhancement of high-entropy bulk metallic glasses by electroless plating with Ni-P amorphous films, Mater. Sci. Eng. A 673 (2016) 141–147.